Non-Faradaic Electrochemical Modification of the Catalytic Activity of Pt for H 2 Oxidation in Aqueous Alkaline Media

ARTICLE *in* THE JOURNAL OF PHYSICAL CHEMISTRY · AUGUST 1996

Impact Factor: 2.78 · DOI: 10.1021/jp960971u

5 AUTHORS, INCLUDING:

Stylianos G. Neophytides
Foundation for Research and Technology - H…
159 PUBLICATIONS **3,044** CITATIONS

SEE PROFILE

Dimitrios Tsiplakides
Aristotle University of Thessaloniki
51 PUBLICATIONS **893** CITATIONS

SEE PROFILE

M. M. Jaksic
University of Belgrade
100 PUBLICATIONS **1,521** CITATIONS

SEE PROFILE

C. G. Vayenas
University of Patras
315 PUBLICATIONS **6,865** CITATIONS

SEE PROFILE

Non-Faradaic Electrochemical Modification of the Catalytic Activity of Pt for H_2 Oxidation in Aqueous Alkaline Media

S. G. Neophytides, D. Tsiplakides, P. Stonehart,† M. Jaksic,‡ and C. G. Vayenas*

Department of Chemical Engineering, University of Patras, Patras GR-26500, Greece

Received: April 2, 1996; In Final Form: June 10, 1996[⊗]

The heterogeneous catalytic oxidation of H_2 on Pt was investigated on Pt black and Pt−graphite electrodes, also serving as heterogeneous catalysts, in aqueous alkaline solutions as a function of electrode potential and current. Hydrogen−oxygen mixtures were bubbled over the surface of the Pt electrode through a porous Teflon frit, and the rates of H_2 and O_2 consumption were measured via on-line mass spectrometry and gas chromatography. It was found that positive current application enhances the catalytic rate of H_2 oxidation by up to 500% and that the increase in the catalytic rate is up to 100 times larger than the increase $I/2F$ of the electrocatalytic rate corresponding to Faraday's law. The results show that the heterogeneously catalyzed H_2 oxidation proceeds in parallel with the electrocatalytic anodic H_2 oxidation and that its rate is markedly affected by the catalyst potential and work function. This electrochemically induced and controlled reversible promotion of the catalytic properties of Pt bears many similarities to the effect of electrochemical promotion when using solid electrolytes and can be rationalized by considering the effect of varying potential and work function on the coverages and binding strengths of dissociatively chemisorbed hydrogen and oxygen.

1. Introduction

Electrochemical promotion of the catalytic activity of metals is a new emerging technique to activate and precisely tune the rate and product selectivity of heterogeneous catalytic reactions on metal surfaces.[1−16] This novel phenomenon was first discovered using solid electrolyte galvanic cells of the type:

gaseous reactants (e.g., CO + O_2)	metal (e.g., Pt, Rh, Ag)	solid electrolyte (e.g., $ZrO_2(Y_2O_3)$)	counter electrode, (e.g., Pt)	auxiliary gas (e.g., O_2)

where the metal working electrode also serves as a catalyst for the heterogeneously catalyzed reaction. It was found that by applying currents or potentials (±1−2 V) between the catalyst and the counter electrode, one obtains dramatic non-Faradaic changes in the rates of catalytic reactions. The increase, Δr, in the catalytic rate can be up to a factor of 3×10^5 higher than the rate, $I/2F$, of O^{2-} supply to the catalyst[2,7] and up to 100 times higher than the open-circuit catalytic rate.[14] Pronounced and technologically interesting variations in product selectivity have also been obtained, e.g., in the case of ethylene epoxidation on Ag.[10] The effect has been studied during the last 7 years for more than 30 catalytic reactions on Pt, Pd, Rh, Ag, IrO_2, and Ni surfaces using a variety of solid electrolytes, including O^{2-},[1,2,5,8,13,14] Na^+,[3,6,11,12] F^-,[15] and protonic[4] conductors. Work in this area has been reviewed recently.[7,10,16] Recent TPD,[17] XPS,[18,19] SERS,[20] work function,[3,21] and cyclic voltammetric[22] investigations have confirmed the original hypothesis[2,7] that this novel effect of non-Faradaic electrochemical modification of catalytic activity (NEMCA),[1−10] or electrochemical promotion[23] or in situ controlled promotion,[11] is due to the electrochemically controlled back-spillover (migration) of promoting ionic species ($O^{\delta-}$, $Na^{\delta+}$) from the solid electrolyte to the gas-exposed catalyst−electrode surface. These back-spillover ionic species are formed, upon current application, at the three-phase boundary metal−gas−solid electrolyte and establish an "effective electrochemical double layer"[8,16] on the catalyst surface, altering its work function[3,21] and thus its chemisorptive[17,24] and catalytic[1−23] properties in a pronounced and reversible manner. The importance of NEMCA in heterogeneous catalysis and electrochemistry has been discussed by Pritchard[23] and Bockris,[25] respectively.

The magnitude of the NEMCA effect for different catalytic reactions is described by three parameters.

1. The first parameter is the enhancement factor or Faradaic efficiency, Λ

$$\Lambda = \Delta r/(I/2F) \tag{1}$$

where the catalytic rate change, Δr, is expressed in mol O, or, more generally, g-equivalent in which case $\Lambda = \Delta r/(I/F)$. A reaction exhibits NEMCA when $|\Lambda| > 1$. When $\Lambda \gg 1$ or $\Lambda \ll -1$, the reaction is termed electrophobic or electrophilic, respectively. Λ values up to 3×10^5 have been measured.[2,7] A major step in the elucidation of the origin of NEMCA was the observation that the order of magnitude of $|\Lambda|$ can be predicted for any catalytic reaction, catalyst, or solid electrolyte from[7,10,16]

$$|\Lambda| \approx 2Fr_o/I_o \tag{2}$$

where I_o is the exchange current of the metal−solid electrolyte interface.

2. The second parameter is the rate enhancement ratio ρ,

$$\rho = r/r_o \tag{3}$$

where r and r_o are the NEMCA-induced and open-circuit catalytic rates, respectively. ρ values up to 100 have been measured with O^{2-} conductors,[14] while even higher values, approaching "infinity", have been recently reported with Na^+ conductors.[12]

3. The third parameter is the promotion index P_i,

$$P_i = \frac{\Delta r/r_o}{\Delta \theta_i} \tag{4}$$

where θ_i is the coverage of the promoting ionic species ($Na^{\delta+}$,

† Stonehart Associates, Connecticut.
‡ Present address: University of Belgrade.
* Corresponding author. Fax: (00) 30-61-997269.
[⊗] Abstract published in *Advance ACS Abstracts,* August 1, 1996.

S0022-3654(96)00971-9 CCC: $12.00

$O^{\delta-}$) on the catalyst surface. $P_{Na^{\delta+}}$ values up to 250 [11] and $P_{O^{\delta-}}$ values up to 100 [14] have been measured.

There had been two early reports of non-Faradaic rate enhancements in aqueous electrochemistry.[26−28] Despic and coworkers found a significant enhancement in the time-averaged rate of ester hydrolysis on a Pt electrolyte subject to cyclic voltammetric treatment.[26] Although the time-averaged absolute Faradaic efficiency $\bar{\Lambda}$, which we define from

$$\bar{\Lambda} = \frac{\oint \Delta r \, dt}{\oint (|I|/2F) \, dt} \tag{5}$$

was below unity in that study, the time-averaged enhancement factor $\bar{\Lambda}^*$, which we define from

$$\bar{\Lambda}^* = \frac{\oint \Delta r \, dt}{\oint (I/2F) \, dt} \tag{6}$$

was obviously very large and approached infinity, since the denominator in eq 6 vanishes during the cyclic voltammetric experiments while the numerator, interestingly, remained positive.

A steady-state Λ value exceeding unity ($\Lambda = 2$) was obtained for the production of H_2 during the investigation of formaldehyde oxidation on Cu[27] and Ag[28] electrodes in alkaline aqueous solution. These findings were attributed to a potential-dependent catalytic step in agreement with the theory of NEMCA in solid electrolyte systems.[28]

Very recently, the NEMCA effect was demonstrated clearly for the first time in aqueous electrolyte media for the $H_2 + O_2$ reaction over a Pt−graphite catalyst−electrode in contact with 0.1 M KOH and 0.1 M LiOH aqueous electrolyte at room temperature.[29] Steady-state Faradaic efficiency Λ values up to 20 and ρ values up to 5 were obtained.[29]

In the present work we report on a systematic study of H_2 oxidation on Pt−graphite and Pt black electrodes and examine the effect of gaseous composition and flow rate, temperature, and electrolyte composition on the NEMCA behavior of the system.

2. Experimental Section

Figure 1 shows the apparatus. It consists of the gas feed unit, the electrochemical cell reactor, and the analysis unit, which comprises on-line gas chromatography and mass spectrometry for reactant and product analysis.

Reactants were Air Liquide certified standards of H_2 and O_2 in He, which could be further diluted with ultrapure (99.999%) He.

A Perkin-Elmer Sigma 300 gas chromatograph (GC) with an HP 3395 integrator and a molecular sieve 5A packed column (80/100 mesh, 10 ft × 1/8 in. at 80 °C) was used to separate and analyze O_2 and H_2. Reactant and product gas samples were injected into the GC unit using a six-port valve with a 1 cm^3 sampling loop, while a four-port valve was used to switch between reactants and products (Figure 1). Water vapor in the products was trapped in a silica gel trap.

The H_2 and O_2 mole fractions in the exit stream, y_{H_2} and y_{O_2}, respectively, were also monitored via on-line mass spectrometry (Figure 1) using a Balzers QMG 311 mass spectrometer equipped with a GES 010 Balzers continuous gas-sampling system.

The rates of H_2, O_2, and atomic oxygen O consumption (r_{H_2}, r_{O_2}, and r_O, respectively), expressed in mol/s, are computed from the outlet H_2 and O_2 mole fractions y_{H_2} and y_{O_2} via

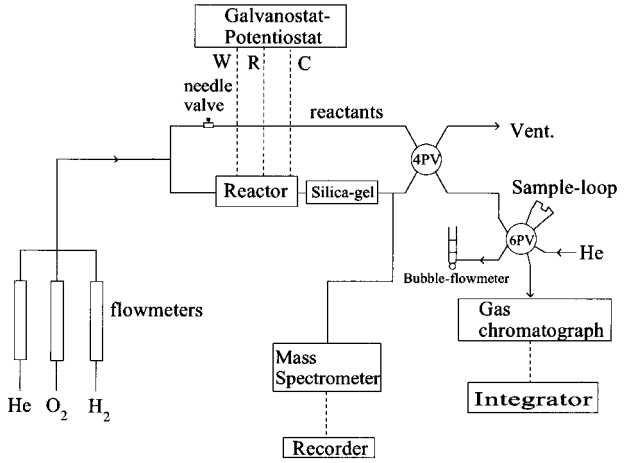

Figure 1. Schematic diagram of the experimental setup.

$$r_{H_2} = f_m(y_{H_2,in} - y_{H_2}) \tag{7}$$

$$r_O = 2r_{O_2} = 2f_m(y_{O_2,in} - y_{O_2}) \tag{8}$$

where $y_{H_2,in}$ and $y_{O_2,in}$ are the inlet mole fractions of H_2 and O_2 and f_m is the total molar flow rate (mol/s). The latter is practically identical (within 0.4%) in the reactor inlet and outlet, owing to the low $y_{H_2,in}$ and $y_{O_2,in}$ values used (<0.02) and the intentionally low conversion of H_2 and O_2 (<20%) in order to operate the cell reactor as a differential reactor.[7,29] The H_2 and O_2 conversion was kept to these low levels by maintaining the total volumetric flow rate f_V in the range 100−800 mL/min, thus the total molar flow rate f_m in the range 0.75×10^{-4} to 6×10^{-4} mol/s. Over this range, changing the flow rate was found to have no significant effect on the rate of consumption of hydrogen and oxygen. This shows the absence of any significant mass transfer limitations for the catalytic reaction.

The atmospheric pressure continuous flow electrochemical cell reactor is shown in Figure 2. The thermostatted glass vessel (volume 0.5 L) was almost completely filled with 0.01−0.5 M KOH or LiOH aqueous solution to minimize dead gas volumes.

Two types of working catalyst-electrodes were used. (1) One type was porous Pt black deposited on a Teflon frit (Stonehart Associates, superficial surface area 2 cm^2). The total surface area of the Pt black sample was 2100 cm^2, corresponding to 2.3×10^{18} surface Pt atoms or 3.84×10^{-6} surface Pt mols. (2) The second type was finely dispersed Pt on graphite, supported again on a Teflon frit (Stonehart Associates, 20 wt % Pt on a graphite superficial surface area of 3.8 cm^2). Its total Pt surface area was 1200 cm^2, corresponding to 1.3×10^{18} surface Pt atoms or 2.2×10^{-6} mol of surface Pt.

The gas mixture was supplied to the Teflon-frit supported Pt catalyst via a glass tube attached to a Plexiglass catalyst holder (Figure 2b). The entire assembly was immersed in the solution, and the gas mixture was sparged through the Teflon catalyst-support frit (thickness ≈ 50 μm).

The catalyst−electrode potential was measured with respect to a reference hydrogen electrode (r.h.e.) using a Luggin capillary (Figure 2b). The Pt counter electrode was enclosed in a glass tube (Figure 2a) so that gases produced or consumed at the counter electrode could not interfere with the main gas stream. Constant currents I between the catalyst and counter electrode and constant potentials E between the catalyst and reference electrodes were applied using an AMEL 553 galvanostat-potentiostat.

3. Results

NEMCA: A Galvanostatic Transient. Figure 3 shows a typical galvanostatic transient obtained with the Pt−graphite

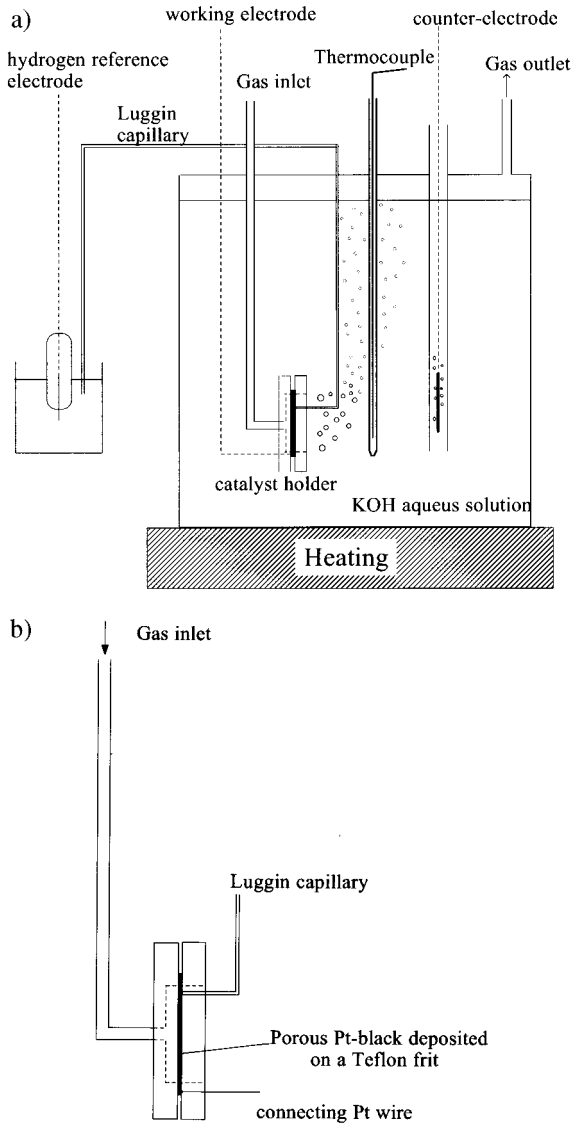

Figure 2. (a) Electrochemical reactor cell; (b) catalyst holder assembly.

catalyst−electrode. The figure depicts the transient response of the rates of H_2 and atomic oxygen consumption, r_{H_2} and r_O ($=2r_{O_2}$), respectively, and of the working electrode−catalyst potential E_{rhe} upon galvanostatic imposition of a positive and of a negative current I. The gaseous inlet H_2 and O_2 mole fractions are $y_{H_2,in} = 1.06 \times 10^{-2}$ and $y_{O_2,in} = 0.75 \times 10^{-2}$ ($P_{H_2} = 1.06$ kPa, $P_{O_2} = 0.75$ kPa), respectively. The volumetric flowrate is $f_v = 280$ mL STP/min.

As shown in the figure, under open-circuit conditions ($I = 0$, $t < 0$), H_2 and O_2 are consumed at a rate

$$r^\circ_{H_2} = r^\circ_O = 2.3 \times 10^{-7} \text{ mol/s} \tag{9}$$

This is due to the catalytic (no net charge transfer) reaction

$$H_2 + (1/2)O_2 \xrightarrow{r_c} H_2O \tag{10}$$

which is catalyzed by the Pt−graphite electrode surface and proceeds at a rate $r^\circ_c = r^\circ_{H_2} = r^\circ_O$.

The open-circuit catalyst potential E°_{rhe} with respect to the reference hydrogen electrode (rhe) is 0.69 V.

A $t = 0$, a constant positive current I is applied between the Pt−graphite catalyst−electrode and the Pt counter electrode (Figure 3). The catalyst potential E_{rhe} changes to more positive values, and the rates of H_2 and oxygen consumption, r_{H_2} and r_O, increase by 344% and 310%, respectively, with respect to

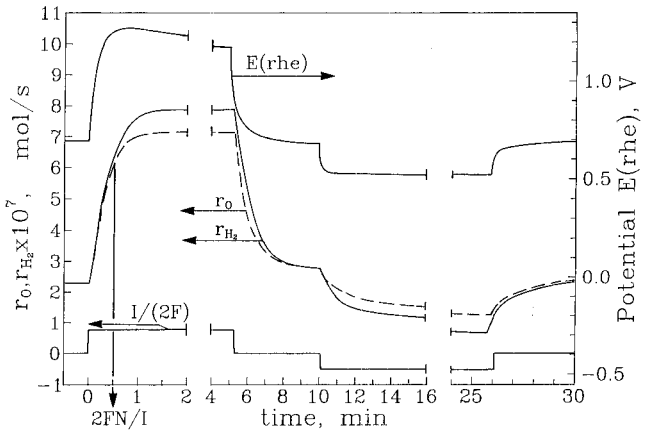

Figure 3. Transient effect of applied positive and negative currents ($I = +15$ and -10 mA) on the rate of consumption of hydrogen (r_{H_2}) and oxygen (r_O): $P_{O_2} = 1.06$ kPa; $P_{H_2} = 0.75$ kPa; gas flow rate $f_v = 280$ cm^3 min^{-1} at STP.

their initial values (Figure 3). The rate increase in H_2 consumption ($\Delta r = 5.6 \times 10^{-7}$ mol H_2/s) is 720% higher than $I/2F$ ($=7.8 \times 10^{-8}$ mol/s). Thus, each OH^- supplied to the catalyst causes the oxidation of about seven H atoms originating from gaseous H_2. Consequently, the Faradaic efficiency Λ defined from

$$\Lambda = \frac{\Delta r_{H_2}}{I/2F} \tag{1}$$

is 7.2 for the galvanostatic experiment of Figure 3.

It is worth noting in Figure 3 that during current application it is $r_{H_2} \neq r_O$ and in fact

$$r_{H_2} - r_O = I/2F \tag{11}$$

Equation 11 holds both for positive and for negative currents (Figure 3). This can be explained directly as follows. There are two electrocatalytic (charge transfer) reactions taking place at the working electrode:

$$H_2 + 2OH^- \xrightarrow{r_{e,1}} 2H_2O + 2e^- \tag{12}$$

$$2OH^- \xrightleftharpoons{r_{e,2}} (1/2)O_2 + H_2O + 2e^- \tag{13}$$

Reaction 12 proceeds to the right at a rate $r_{c,1} > 0$ as long as $E_{rhe} > 0$, which was always the case in the present work. Reaction 13 proceeds to the right ($r_{e,2} > 0$) when E_{rhe} exceeds the oxygen reduction potential (1.23 V) and to the left ($r_{e,2} < 0$) otherwise. In either case it follows from simple mass and electron balance considerations that

$$r_{H_2} = r_c + r_{e,1} \tag{14}$$

$$r_O = r_c - r_{e,2} \tag{15}$$

$$I/2F = r_{e,1} + r_{e,2} \tag{16}$$

Combining eqs 9−11 one obtains

$$r_{H_2} - r_O = I/2F \tag{11}$$

which is in excellent agreement with the experimental results both for positive and for negative currents (Figure 3).

It follows from eq 16 that when $I = 0$, then $r_{e,2} = -r_{e,1}$. Therefore, the open-circuit conditions E°_{rhe} is a mixed potential bounded between 0 and 1.23 V. We then apply eqs 14−16

and 11 between the final state ($I = I$) and the initial state ($I = 0$) of the first galvanostatic experiment of Figure 3:

$$\Delta r_{H_2} = \Delta r_c + \Delta r_{e,1} \quad (14a)$$

$$\Delta r_O = \Delta r_c - \Delta r_{e,2} \quad (15a)$$

$$I/2F = \Delta r_{e,1} + \Delta r_{e,2} \quad (16a)$$

$$I/2F = \Delta r_{H_2} - \Delta r_O \quad (11a)$$

Since both the forward reactions 12 and 13 are anodic, it follows that a positive I, causing an increase in catalyst potential E_{rhe}, will also cause an increase in both $r_{e,1}$ and $r_{e,2}$, i.e., $\Delta r_{e,1} > 0$ and $\Delta r_{e,2} > 0$. Consequently, if the rate of the catalytic reaction, r_c, were changing upon current application ($\Delta r_c = 0$) it follows from eq 15a that

$$\Delta r_O < 0 \quad (17)$$

and from eq 11a that

$$\Delta r_{H_2} < I/2F \quad (18)$$

On the contrary, as shown in Figure 3 at steady state, it is

$$\Delta r_O = (6.2)(I/2F) \quad (19)$$

$$\Delta r_{H_2} = (7.2)(I/2F) \quad (20)$$

This shows conclusively that r_C has changed substantially upon current application. In fact, in view of eqs 14a and 15a one has

$$(6.2)(I/2F) < \Delta r_c < (7.2)(I/2F) \quad (21)$$

or, more generally

$$\Lambda_O(I/2F) < \Delta r_c < \Lambda_{H_2}(I/2F) \quad (22)$$

where the Faradaic efficiencies Λ_{H_2} and Λ_O are defined, as usually, from

$$\Lambda_{H_2} = \frac{\Delta r_{H_2}}{(I/2F)}; \quad \Lambda_O = \frac{\Delta r_O}{(I/2F)}; \quad \Lambda_{H_2} - \Lambda_O = 1 \quad (1)$$

Consequently, the observed non-Faradaic rate enhancement is due to the acceleration of the *catalytic* rate of H_2 oxidation.

As also shown in Figure 3, the rate relaxation time constant τ, defined as the time required for the rate increase to reach 63% of its steady-state value during a galvanostatic transient is found to be 60 s, in good qualitative agreement with the parameter $2FN/I$ (=30 s), which is the time required to form a monolayer of adsorbed atomic oxygen over the entire Pt surface. This is a general observation also in NEMCA studies using solid electrolytes.[1−24]

Upon current interruption r_{H_2}, r_O, and E_{rhe} return to their open-circuit values (Figure 3). The effect is thus quite reversible. Negative current application also causes a decrease in r_{H_2} and r_O, which is larger than $|I/2F|$. It is worth noting that eq 11 holds again at steady state.

As previously noted, the Pt counter electrode wire (2 mm in diameter) was enclosed in a glass tube (Figure 2a) so that gases (H_2 or O_2) produced or consumed there could not interfere with the gas stream flowing through the working electrode. The charge transfer reactions taking place at the Pt counter electrode are the reverse of reactions 12 and 13, i.e., H_2 evolution when the potential, E'_{rhe}, of the counter electrode is negative, oxygen evolution when $E'_{rhe} > 1.23$ V, and oxygen reduction when $E'_{rhe} < 1.23$ V.

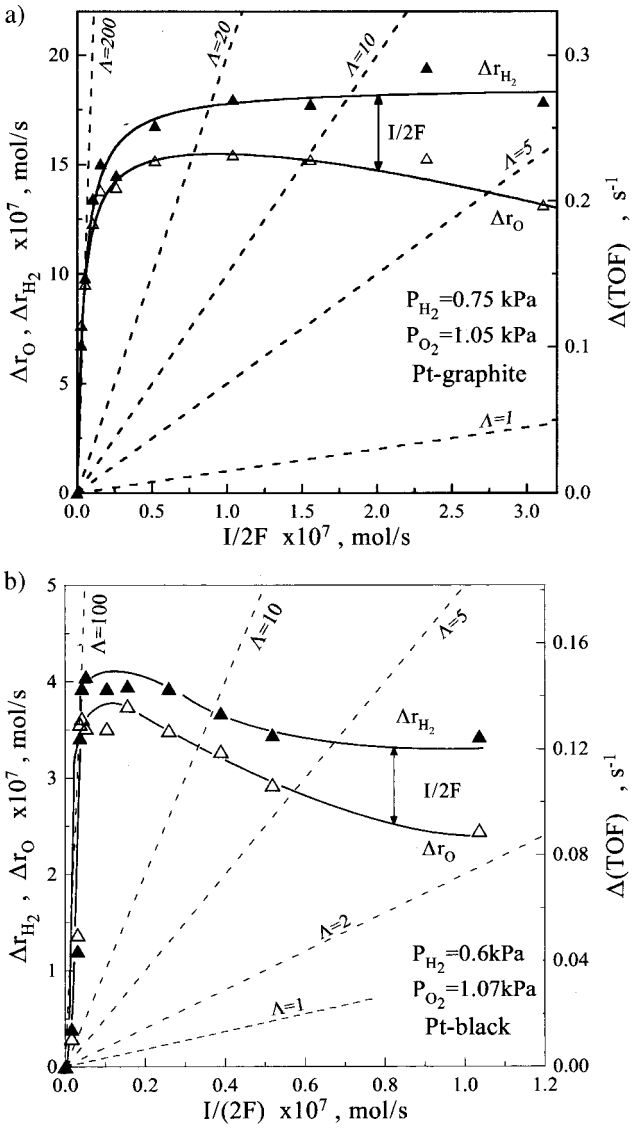

Figure 4. Steady-state effect of applied positive current on the increase in the consumption rates of H_2 (▲) and O_2 (Δ): (a) Pt−graphite 0.1 M KOH, $r_C^o = r_{H_2}^o = r_O^o = 7.71 \times 10^{-7}$ mol/s, $f_m = 36 \times 10^{-5}$ mol/s; (b) Pt black 0.1 M KOH, $r_C^o = r_{H_2}^o = r_O^o = 1.94 \times 10^{-7}$ mol/s, $f_m = 3.2 \times 10^{-6}$ mol/s.

Steady-State Effect of Current. Parts a and b of Figure 4 show the steady-state effect of applied current I on $\Delta r_{H_2}(=r_{H_2} - r_{H_2}^o)$ and $\Delta r_O(=r_O - r_O^o)$, where the superscript "o" always denotes open-circuit conditions, for Pt−graphite and Pt black electrodes. The Faradaic efficiency, Λ, is for both catalysts of the same order of magnitude and exceeds 100 (10 000%) for low currents. In both cases increasing current causes a decrease in Λ. As shown in Table 1, the measured maximum Λ values are for both catalysts in good qualitative agreement with the approximate equation

$$|\Lambda| \approx 2Fr_c^o/I_o \quad (2)$$

where I_o is the exchange current of the catalyst−electrolyte interface extracted from current−overpotential plots in the presence of the H_2-O_2 mixture. Equation 2 has been derived elsewhere[7] and has been shown to predict the order of magnitude of the absolute value of Λ in solid electrolyte NEMCA studies.[1−22] It shows that a necessary condition for obtaining $|\Lambda|$ values above unity is that the open-circuit *catalytic* rate r_c^o must be higher than the exchange *electrocatalytic* rate $I_o/2F$.

TABLE 1: Catalyst−Electrode Properties, Measured Open-Circuit Turnover Frequencies (TOF) at P_{H_2} = 0.75 kPa and P_{O_2} = 1.05 kPa, and Measured and Predicted (Eq 2) Faradaic Efficiency Λ Values for Two Pt−Graphite and One Pt Black Catalyst

catalyst	electrol.	$r_c^o \times 10^7$ mol/s	I_o mA	$\lvert\Lambda_{exp}\rvert$	$\lvert\Lambda_{pred.}\rvert = 2Fr_c^o/I_o$	N_{Pt}	TOF/s^{-1}
Pt−gr$_1$	0.1 M KOH	7.7	0.75	184	199	2.2×10^{-6}	0.35
Pt−gr$_2$	0.1 M LiOH	1.8	0.26	25	133	2.2×10^{-6}	0.08
Pt−bl	0.1 M KOH	1.9	0.27	80	135	3.8×10^{-6}	0.05

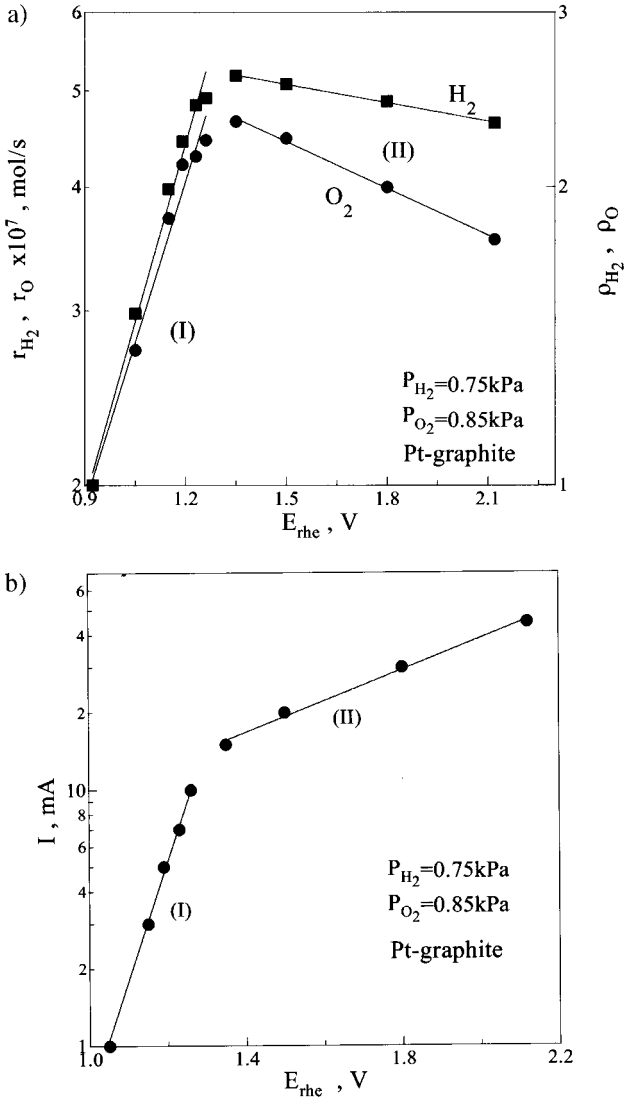

Figure 5. Steady-state effect of catalyst potential, E_{rhe}, on the consumption rates of hydrogen and oxygen (a) and on the current, I, (b). Pt−graphite is in 0.1 M LiOH; $f_m = 18.75 \times 10^{-5}$ mol/s.

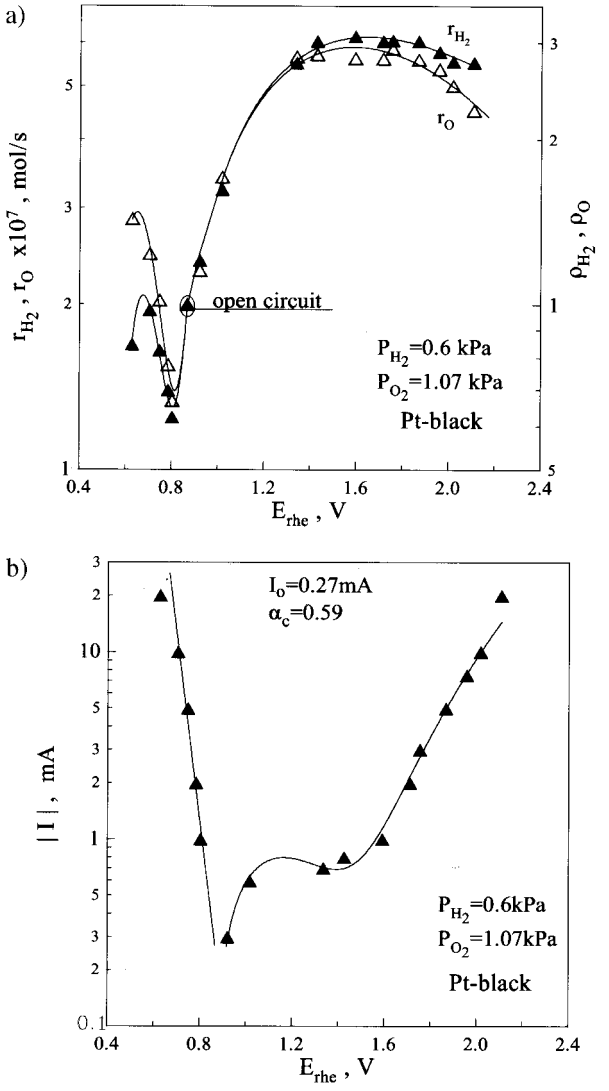

Figure 6. Steady-state effect of catalyst potential, E_{rhe}, on the consumption rates of hydrogen and oxygen (a) and on the absolute value $|I|$ of the current, I, (b). Current is negative for $E_{rhe} < 0.86$ V. Pt black is in 0.1 M KOH; $f_m = 3.2 \times 10^{-6}$ mol/s.

Table 1 also shows computed turnover frequencies (TOF) under standard P_{H_2} and P_{O_2} conditions. In catalysis TOF (s^{-1}) is defined as molecules (of H_2) reacting per surface catalyst (Pt) atom per second.

Effect of Catalyst Potential E_{rhe}. Previous NEMCA studies using solid electrolytes have shown the central role of catalyst−electrode potential in describing this novel effect.[1−22] The notation V_{WR} has been used in solid electrolyte NEMCA studies to denote the catalyst (working electrode, W) potential with respect to the reference (R) electrode. The main conclusion derived from previous NEMCA studies is that over wide ranges of catalyst potential and work function, which can be controlled potentiostatically by varying the IR-free catalyst potential,[3,7] catalytic rates, r, depend exponentially on catalyst potential and work function $e\Phi$:

$$\ln(r/r_o) = \alpha(V_{WR} - V^*_{WR})/k_bT = \alpha(e\Phi - e\Phi^*)/k_bT \quad (19)$$

where α, V^*_{WR}, and $e\Phi^*$ are reaction and catalyst specific constants. The parameter α termed "NEMCA coefficient" (positive for electrophobic reactions, negative for electrophilic ones) usually takes a value between −1 and 1.

As shown in Figures 5a and 6a, similar trends hold here for the Pt−graphite as well as for the Pt black catalysts in the region 0.9 V < E_{rhe} < 1.2 V where the rates of H_2 and O_2 consumption increase exponentially with E_{rhe} with α values on the order of 0.06 (electrophobic behavior).

In the case of the Pt−graphite electrode the rate maximum at $E_{rhe} \approx 1.25$ V is accompanied by a break in the ln I vs E_{rhe} plot (Figure 5b). This break in the Tafel plot and corresponding catalytic rate maximum (Figure 5a) take place in the region of the completion of surface Pt oxide formation and onset of gaseous O_2 evolution.[30−33]

In the case of the Pt black electrode (Figure 6) the formation of surface Pt oxide is clearly manifested by the inflection point in the ln I vs E_{rhe} plot (Figure 6b). The catalytic rate increases

exponentially over the Pt oxide formation region (Figure 6a) and starts to decrease in the region of O_2 evolution (Figures 5a and 6a).

In the case of the Pt black electrode the effect of negative currents ($I < 0$, $E_{rhe} < E^{\circ}_{rhe}$) was also investigated (parts a and b of Figure 6). Interestingly, the rates go through a minimum to the left of the open-circuit potential E°_{rhe} followed by the appearance of a second rate maximum at more negative potentials (Figure 6a).

Figure 7a shows the effect of catalyst potential $E_{rhe}(>E^{\circ}_{rhe})$ on the rate enhancement ratio ρ of H_2 oxidation for fixed P_{H_2} and four different values of P_{O_2}. The rate enhancement ratio ρ increases from 1.5 to 4 as P_{O_2} increases from 0.29 to 1.5 kPa, i.e., the rate increase is more pronounced for high P_{O_2}/P_{H_2} ratios.

Electrocatalytic Performance in H_2 and O_2 Environments. In two separate sets of experiments we obtained current−potential curves of the Pt−graphite catalyst electrode at $P_{H_2} = 0.8$ kPa in the absence of oxygen (curve labeled "$r_{H_2,H_2\ feed}$" in Figure 7b, bottom) and at $P_{O_2} = 1.17$ kPa in the absence of H_2 (curve labeled "$r_{O,O_2\ feed}$" in Figure 7b, bottom). Figure 7b, as in previous figures, shows rates of H_2 and O_2 consumption. Consequently, H_2 and O_2 evolution rates appear as negative rates in the figure.

In a third experiment H_2 and O_2 were cofed over the same Pt−graphite catalyst−electrode using the same previous partial pressures ($P_{H_2} = 0.8$ kPa, $P_{O_2} = 1.17$ kPa) and the effect of catalyst potential on the rates of consumption of H_2 and O_2 (curves labeled "$r_{H_2,mixed\ feed}$" and "$r_{O,mixed\ feed}$" in Figure 7b, top) and on the total electrocatalytic rate $I/2F$ (Figure 7b top *and* bottom) was examined. Note that the curves labeled "$r_{H_2,mixed\ feed}$" and "$r_{O,mixed\ feed}$" always differ by $I/2F$. They cross each other under open-circuit conditions ($I = 0$).

The curves labeled "$r_{H2,H_2\ feed}$" and "$r_{O,O_2\ feed}$" in Figure 7b shows the rates of consumption of H_2 and O_2, respectively, according to the charge transfer reactions 12 and 20, which is the reverse of reaction 13, i.e.,

$$H_2 + 2OH^- \rightarrow 2H_2O + 2e^- \qquad (12)$$

$$(1/2)O_2 + H_2O + 2e^- \rightarrow 2OH^- \qquad (20)$$

The purpose of these experiments was to examine whether the measured *catalytic* rate of H_2 oxidation (Figure 7b top) might be due to the coupling of reactions 12 and 20 (Figure 7b bottom) in a corrosion-type mechanism.

As shown in Figure 7b bottom, this corrosion-type mechanism (which predicts an open-circuit rate equal to that at the intersection of the "$r_{H_2,H_2\ feed}$" and "$r_{O,O_2\ feed}$" curves in Figure 7b bottom) can account for less than 30% of the measured open-circuit catalytic rate r°_c (Figure 7b, top). This is, in fact, a conservative estimate, since under catalytic (mixed feed) conditions the electrocatalytic rates of H_2 and O_2 consumption are expected to be hindered owing to the coadsorption of O and H, respectively, on the Pt electrode. This must also be the reason for the fact that the "$r_{H_2,H_2\ feed}$" and "$r_{O,O_2\ feed}$" curves do not intersect exactly at the open-circuit potential obtained with the mixed H_2-O_2 feed but at a 0.1 V less positive potential (Figure 7b).

As also shown in Figure 7b, O_2 consumption (evolution) takes place above 1.3 V whereas net oxygen consumption takes place over the same potential range under mixed H_2-O_2 feed concitions. It may thus be safely concluded on the basis of Figure 7b that the measured catalytic rate is not due to a corrosion-type mechanism involving net charge-transfer reactions but proceeds via chemisorbed hydrogen and oxygen intermediates, i.e., the reaction mechanism is catalytic and is not due to the coupling of two electrocatalytic reactions.

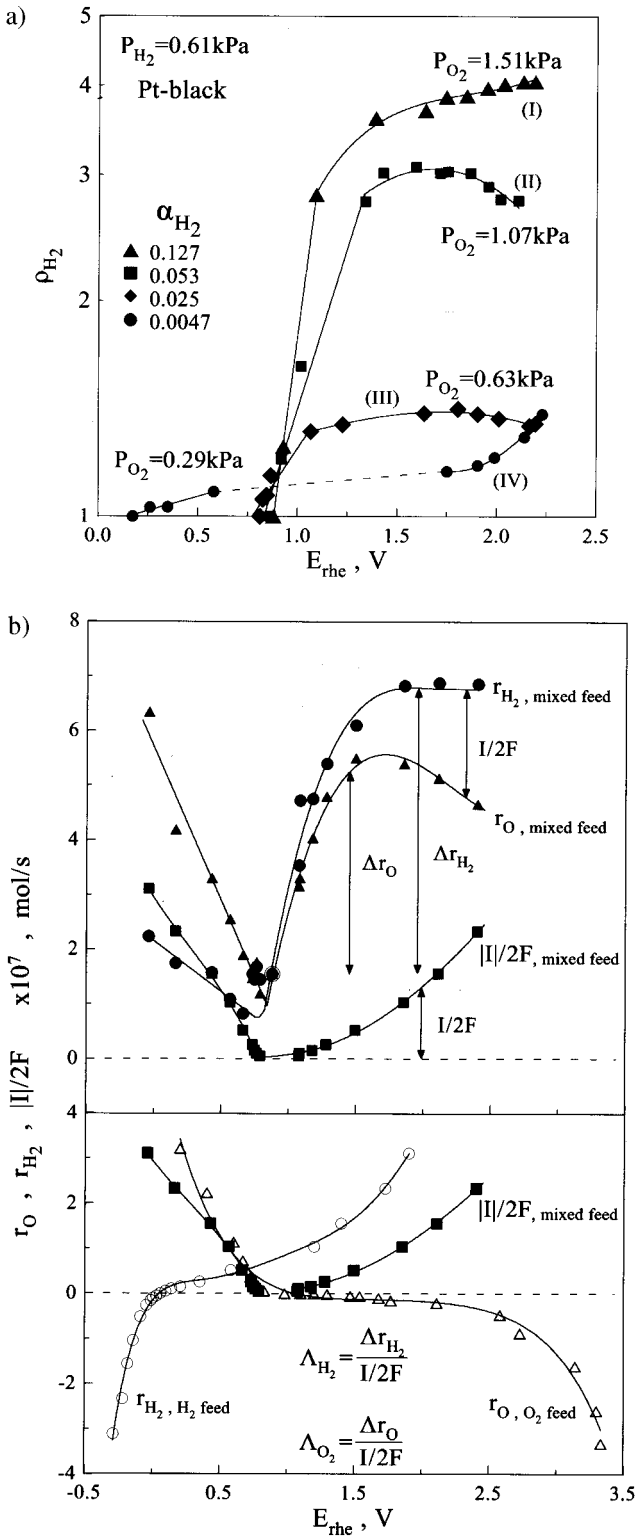

Figure 7. (a) Effect of catalyst potential, E_{rhe}, on the rate enhancement ratio, $\rho_{H_2} = r_{H_2}/r^{o}_{H_2}$, of H_2 oxidation for fixed P_{H_2} and various P_{O_2} values: (I) $r^{o}_{H_2} = 1.17 \times 10^{-7}$ mol/s; (II) $r^{o}_{H_2} = 2.03 \times 10^{-7}$ mol/s; (III) $r^{o}_{H_2} = 5.22 \times 10^{-7}$ mol/s; (IV) $r^{o}_{H_2} = 3.53 \times 10^{-7}$ mol/s. $f_m = 33 \times 10^{-5}$ mol/s; Pt black is in 0.1 M KOH. (b) Effect of catalyst potential, E_{rhe}, on the rates of H_2 (●) and O_2 (▲) consumption (top) and on the absolute value $|I|$ of the current I (■) (top and bottom) when H_2 and O_2 are cofed ($P_{H_2} = 0.8$ kPa, $P_{O_2} = 1.17$ kPa) over the catalyst−electrode (top) and on the electrocatalytic rates of H_2 (○) and O_2 (△) consumption when they are fed separately at the same partial pressures over the same catalyst−electrode (bottom). Pt−graphite is in 0.1 M KOH, and the circled solid circle is the open circuit rate $r^{o}_c = r^{o}_{H_2} = r^{o}_O = 1.5 \times 10^{-7}$ mol/s.

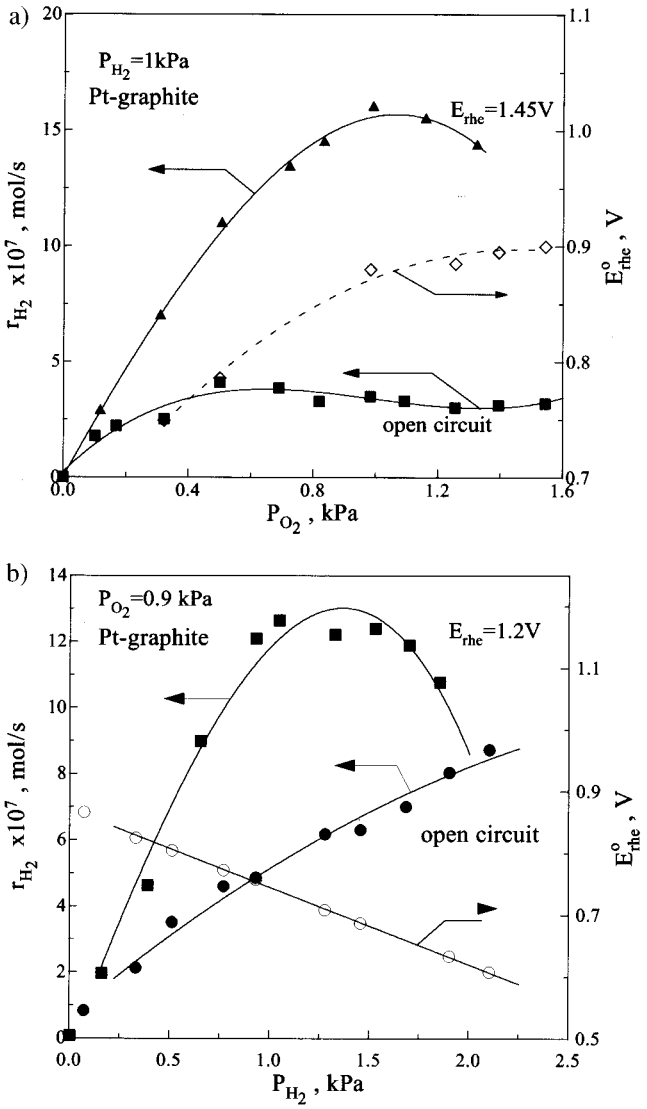

Figure 8. Effect of P_{O_2} (a) ($f_m = 22 \times 10^{-5}$ mol/s) and P_{H_2} (b) ($f_m = 35 \times 10^{-5}$ mol/s) on the rate of H_2 oxidation and corresponding catalyst potential, E^o_{rhe}, under open circuit and on the rate of H_2 oxidation under closed-circuit at fixed catalyst potential, E_{rhe}. Pt−graphite is in 0.1 M LiOH.

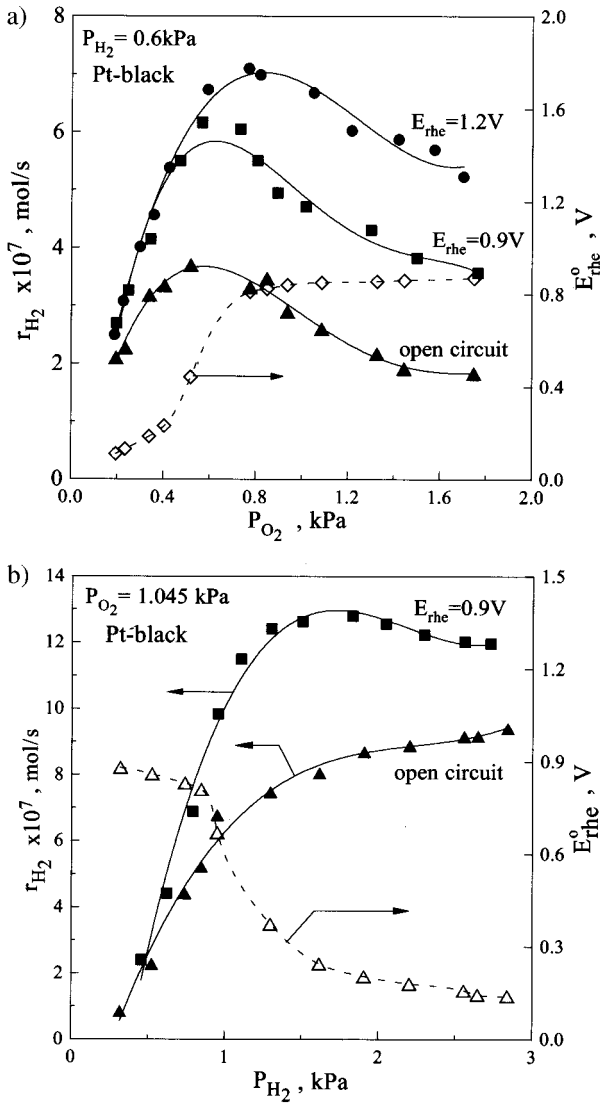

Figure 9. Effect of P_{O_2} (a) and P_{H_2} (b) on the rate of H_2 oxidation and corresponding catalyst potential, E^o_{rhe}, under open circuit and on the rate of H_2 oxidation under closed-circuit at fixed catalyst potential, E_{rhe}. Pt black is in 0.1 M KOH; $f_m = 30 \times 10^{-5}$ mol/s.

The pronounced non-Faradaic nature of the rate increases Δr_{H_2} and Δr_O is also clearly manifested in Figure 7b top, by comparing these parameters with $I/2F$.

Open- and Closed-Circuit Kinetics. In order to examine the origin of the observed non-Faradaic rate enhancement, we have investigated the kinetics of H_2 oxidation on the Pt−graphite and Pt black catalysts first under open-circuit and then under closed-circuit conditions.

The kinetics of H_2 oxidation on Pt at room temperature have been the subject of several previous investigations[34−40] and references therein. All authors agree that the kinetics can be described within the general framework of the classical Langmuir−Hinshelwood kinetic model involving dissociatively chemisorbed H_{ad} and O_{ad} species, which form OH_{ad} in the rate-limiting step of the catalytic reaction. Thus, to a first approximation, the kinetics are expected to obey the following Langmuir−Hinshelwood equation:

$$r = K_R \frac{K_O K_H P_{O_2}^{1/2} P_{H_2}^{1/2}}{(1 + K_O P_{O_2}^{1/2} + K_H P_{H_2}^{1/2})^2} \qquad (21)$$

where K_O and K_H are the dissociative equilibrium adsorption constants for oxygen and hydrogen, which in the present case are expected to be potential-dependent. Equation 21 is indeed in qualitative agreement with the results of open-circuit kinetics shown in Figures 8 and 9 both for the Pt−graphite in 0.1 M LiOH caalyst (Figure 8) and for the Pt black in 0.1 M KOH catalyst (Figure 9). In both cases the *open-circuit* rate exhibits a maximum with respect to P_{O_2} and increases monotonically with P_{H_2}.

Figures 8 and 9 also depict the effect of gaseous composition on the open-circuit catalyst potential E^o_{rhe}. This parameter, bounded between 0 and 1.23 V, is an increasing function of the P_{O_2}/P_{H_2} ratio, yet its exact value is also dependent on the type of electrode used. As shown in Figure 8, E^o_{rhe} varies typically between 0.6 and 0.9 V for the Pt−graphite in 0.1 LiOH catalyst and between 0.15 and 0.9 V for the Pt black in 0.1 M KOH catalyst as the P_{O_2}/P_{H_2} ratio is increased from 0.3 to 4. The latter is also manifested in Figure 7a ($\rho = 1$, i.e., $I = 0$). For fixed P_{O_2}, P_{H_2}, and catalyst type, E^o_{rhe} is practically independent of the cation type (K^+ or Li^+). As previously noted, E^o_{rhe} is basically determined by the mixed potential of the charge-transfer reactions 12 and 20.

It is worth noting that the rate maximum with respect to P_{O_2} is rather shallow in the case of the Pt−graphite catalyst, in which case the increase in E_{rhe} with increasing P_{O_2}/P_{H_2} ratio is also

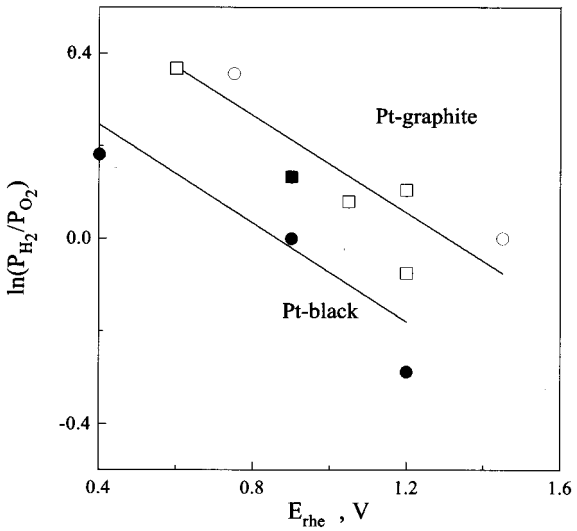

Figure 10. Effect of catalyst potential, E_{rhe}, on the P_{H_2}/P_{O_2} ratio corresponding to the rate maximum with respect to H_2 (squares) and to O_2 (circles). Pt−graphite is in 0.1 M LiOH, and Pt black is in 0.1 M KOH.

quite smooth (Figure 8a). Here, the rate maximum occurs at $P_{O_2}/P_{H_2} \approx 0.5$ and $E_{rhe} \approx 0.78$ V.

In the case of the Pt black catalyst the rate maximum is more pronounced and occurs at $P_{O_2}/P_{H_2} \approx 1$ and $E_{rhe} \approx 0.4$ V while the increase in E_{rhe} with increasing P_{O_2}/P_{H_2} is more abrupt.

It is worth noting that, according to eq 21, the rate maximum with respect to P_{O_2} occurs at

$$K_O P_{O_2}^{1/2} = 1 + K_H P_{H_2}^{1/2};\quad (P_{O_2}/P_{H_2})^{1/2} = (K_H/K_O) + K_O/P_{H_2}^{1/2} \tag{22}$$

while a rate maximum with respect to P_{H_2} is expected at

$$K_H P_{H_2}^{1/2} = 1 + K_O P_{O_2}^{1/2};\quad (P_{O_2}/P_{H_2})^{1/2} = (K_H/K_O) - K_O/P_{H_2}^{1/2} \tag{23}$$

Consequently, the absence of a rate maximum with respect to P_{H_2} (Figures 8b and 9b) reflects the fact that K_H is smaller than K_O under open-circuit conditions, and thus, eq 23 is never satisfied over the P_{O_2}/P_{H_2} range investigated.

Under positive bias conditions, however, the situation changes dramatically. The rate maximum with respect to P_{O_2} shifts to higher P_{O_2} values (Figures 8a and 9a), and more importantly, a rate maximum appears with respect to P_{H_2} (Figures 8b and 9b).

In view of eqs 22 and 23 both observations show a *decrease* in K_O and an *increase* in K_H with increasing E_{rhe}. This implies a weakening in the chemisorptive bond of oxygen and a strengthening in the chemisorptive bond of hydrogen with increasing catalyst potential, in excellent agreement with the theory of electrochemical promotion.[7,16] This is exactly what is expected for an electron acceptor adsorbate (oxygen) and an electron donor adsorbate (hydrogen) upon increasing the catalyst potential and, thus,[3,7,16] the work function.

Figure 10 shows the dependence of the P_{H_2}/P_{O_2} value corresponding to the rate maximum on E_{rhe}. Increasing E_{rhe} causes a pronounced increase in the P_{O_2}/P_{H_2} value corresponding to the rate maximum due to the weakening of the chemisorptive bond of oxygen and the strengthening of the chemisorptive bond of hydrogen. It is worth noting that for the Pt black catalyst the rate maximum with respect to P_{H_2} occurs at higher P_{H_2}/P_{O_2} ratios than the rate maxima with respect to P_{O_2} in good agreement with eqs 22 and 23.

Effect of Flow Rate. Figure 11 shows the effect of varying the total molar and volumetric flow rate, f_m and f_v, respectively, on the catalytic rate of H_2 oxidation on Pt−graphite immersed

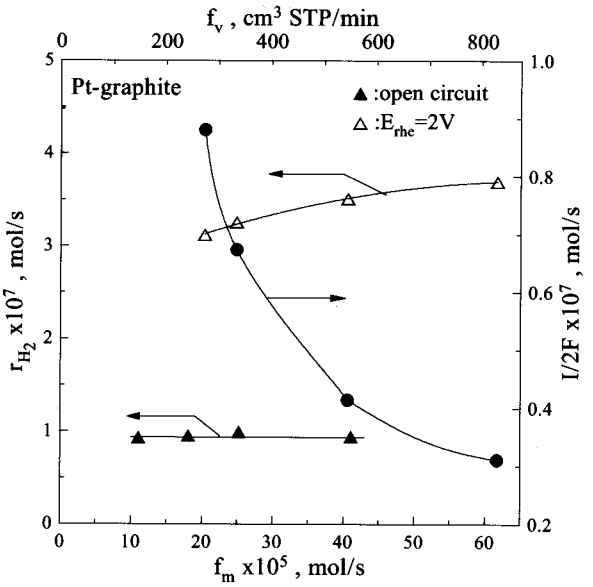

Figure 11. Effect of total molar and volumetric flow rates on the catalytic rate, r_{H_2}, of H_2 oxidation under open-circuit and closed-circuit conditions and on the current, I, corresponding to the closed circuit catalytic rate at fixed potential, E_{rhe}. Pt-graphite is in 0.1 M KOH. P_{O_2} = 1.5 kPa; P_{H_2} = 0.6 kPa.

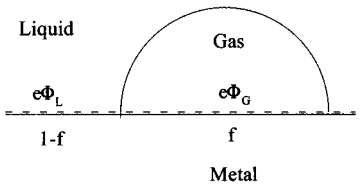

Figure 12. Schematic representation of the gas-exposed fraction (f) and the liquid-exposed fraction ($1 - f$) of the surface area of the gas diffusive catalyst−electrode.

in 0.1 M KOH aqueous solution, both under open-circuit and polarization conditions, for constant P_{O_2} and P_{H_2} values. It is clear that over a wide range of f_v variation, i.e., from 100 to 600 cm^3 STP min^{-1}, the reaction rate remains constant under open-circuit conditions. This experimental observation proves that the measured open-circuit catalytic reaction rate is free of any mass transfer limitations of gaseous reactants, H_2 and O_2, toward the catalytic surface. The measured rate thus expresses the intrinsic catalytic reaction rate of H_2 oxidation on the Pt−graphite catalyst−electrode.

The same applies, within experimental error, to the measured reaction rate under severe polarization conditions. There is only a slight (15%) rate increase as the flow rate is increased by a factor of 3. At the same time the current decreases by a factor of 6 (Figure 11).

These observations, i.e., constancy of catalytic rate and pronounced decrease in electrocatalytic rate, can be explained as follows. Increasing gas flow rate increases the fraction, f, of the gas-exposed catalyst−electrode surface (Figure 12). The electrocatalytic (charge-transfer) rate is proportional to $(1 - f)$. Thus, the current decreases substantially (Figure 11). The catalytic rate, however, takes place over the entire, gas-exposed and liquid-covered, catalyst electrode surface and is thus not significantly affected by changing f. To the extent that there are no mass transfer limitations, the chemical potential of H_2 is the same in the gas phase and in solution. The same applies for O_2. (The thermodynamic activities are also the same if defined using the same standard states, e.g., pure H_2 and pure O_2 at 1 atm.) Consequently, if the rate-limiting step of the catalytic reaction is the surface combination of chemisorbed H_{ad} and O_{ad} (and not the gas adsorption or product desorption steps), it follows that chemisorbed H_{ad} and O_{ad} will be in equilibrium

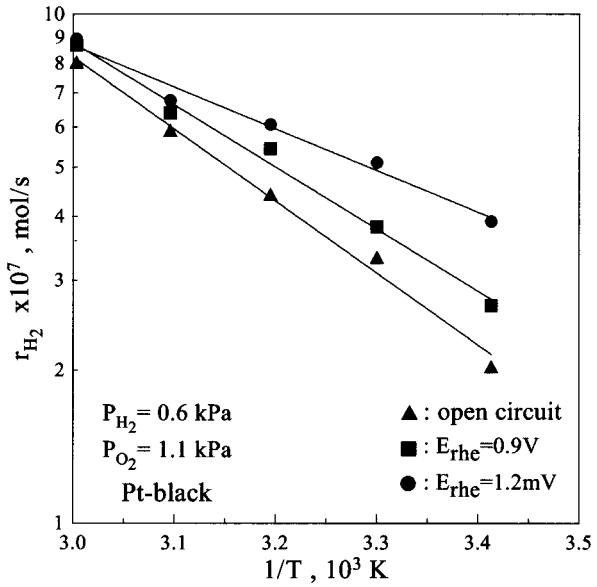

Figure 13. Arrhenius plots under open circuit and at various fixed catalyst potential values E_{rhe}. Pt black is in 0.1 M KOH; $f_m = 32 \times 10^{-5}$ mol/s.

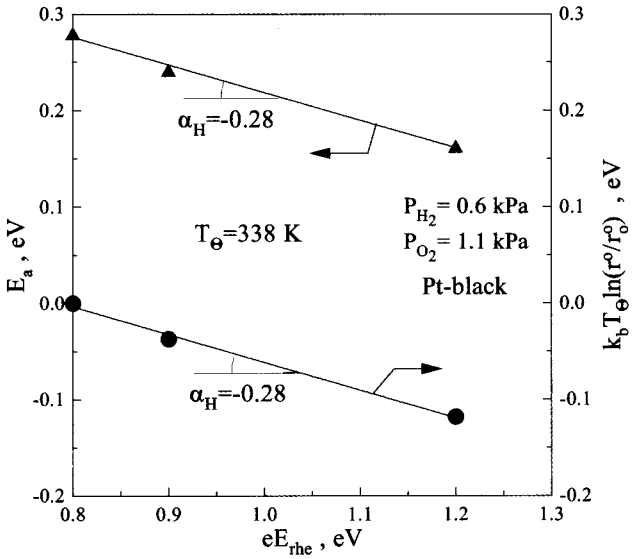

Figure 14. Effect of catalyst potential, E_{rhe}, on activation energy E_a (▲) and preexponential factor, r° (●). r_o°(=0.012 mol H_2/s) is the open-circuit preexponential factor. T_Θ is the isokinetic temperature. Pt black is in 0.1 M KOH.

with gaseous (and dissolved) H_2 and O_2, respectively, and thus will have the same chemical potential both on the liquid-covered and on the gas-exposed electrode surface. Therefore, to the extent that the rate of the surface combination of H_{ad} and O_{ad} is determined by the chemical potentials (or thermodynamic activities) of chemisorbed H_{ad} and O_{ad} rather than by their coverages, which may in general differ in the two regions, it follows that the catalytic rate per unit surface area is expected to be the same in the two regions, in excellent agreement with experimental results (Figure 11). This equal rate assumption is used routinely in the modeling of catalytic hydrogenation reactions on partially wetted catalysts in three-phase reactors. The above observation (Figure 11) shows again that the catalytic reaction proceeds via chemisorbed hydrogen and oxygen adatoms, H_{ad} and O_{ad}, and not via a corrosion-type charge-transfer mechanism, in which case the catalytic rate would follow the electrocatalytic one and would decrease substantially with increasing f.

It is worth noting that the work of Hansen, Kolb, Kötz, and co-workers with emersed electrodes has shown that the double layer structure is retained after electrode emersion as well.[41−44] Consequently, the double layer is expected to exist, more or less, unperturbed over the gas-exposed catalyst electrode surface as well.

Effect of Catalyst Potential, E_{rhe}, on Activation Energy. Compensation Effect. Figure 13 shows Arrhenius plots obtained under open-circuit conditions and for fixed E_{rhe} values at temperatures between 16 and 70 °C. The experiments were carried out under oxidative gas-phase composition ($P_{O_2} = 1.5$ kPa, $P_{H_2} = 0.6$ kPa) where the reaction rate is negative order in O_2 (Figures 8a and 9a). The open circuit catalyst potential, E_{rhe}°, varies from 750 to 800 mV with increasing temperature. The apparent activation energy E_a is 6.45 kcal/mol or 0.28 eV/atom at open-circuit conditions and decreases to 0.12 eV at $E_{rhe} = 1200$ mV with a concomitant pronounced decrease in the preexponential factor r° defined from

$$r = r^\circ \exp(-E_a/RT) \tag{24}$$

It is noteworthy that all three Arrhenius lines converge, providing thus a direct demonstration of the compensation effect[45,46] with an isokinetic point at $T_\Theta = 353$ K.

The compensation effect in heterogeneous catalysis is usually observed for several similar reactions on the same catalyst or for several catalysts and the same reaction.[45,46] In the present case the compensation effect is observed for one reaction and one catalyst via variation of its potential and, thus, work function.[3,44] Although the existence of a true compensation effect in heterogeneous catalysis has been disputed,[46] the present findings, as well as those of previous NEMCA studies,[14,15] clearly demonstrate that the compensation effect is real and constitutes a general feature of electrochemical promotion of catalytic activity.[7,16]

Figure 14 shows that the decrease in activation energy with respect to (eE_{rhe}) is linear with a slope $\alpha_H = -0.28$, defined from

$$E_a = E_a^\circ + \alpha_H \Delta(eE_{rhe}) \tag{25}$$

where E_a° is the open-circuit activation energy value.

It is worth noting that the linear variation of E_a with potential is a common feature in all previous NEMCA studies of catalyst films deposited on solid electrolytes.[2,5,7] This shows that the general features of electrochemical promotion are the same despite the different types of electrolyte used.

Figure 14 also shows that the logarithm of the preexponential factor r° decreases linearly with E_{rhe}, and when $k_b T_\Theta \ln(r^\circ/r_o^\circ)$ (where r_o° is the open-circuit preexponential factor) vs (eE_{rhe}) is plotted, the slope is again −0.28. The difference between the two parallel lines equals the open-circuit activation energy E_a°, as can be shown easily.[14]

According to the above considerations, it is worth noting that the NEMCA effect vanishes at the isokinetic point $T = T_\Theta$. Below the isokinetic point ($T < T_\Theta$) the reaction exhibits electrophobic behavior,[7] i.e., $\partial r/\partial E > 0$ and thus $\alpha > 0$ and $\Lambda > 0$, while electrophilic behavior, i.e., $\partial r/\partial E < 0$, $\alpha < 0$, and $\Lambda < 0$, is expected at temperatures above T_Θ.

Effect of KOH Concentration. Figure 15 depicts the effect of KOH concentration on the rate of H_2 oxidation at open-circuit and under various fixed potentials. The reaction rate decreases with increasing KOH concentration both under open-circuit and under polarization conditions. It is worth noting that the change in catalytic rate, Δr_c, under polarization conditions also decreases with increasing KOH concentration. This shows that the electrolyte concentration is also affecting proportionally the magnitude of the electrochemical enhancement of the catalytic activity.

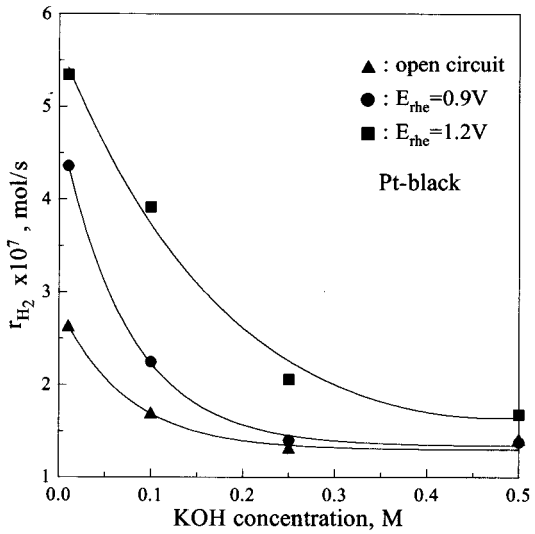

Figure 15. Effect of KOH concentration on the rate of H_2 oxidation both under open circuit and at various fixed potentials: $P_{O_2} = 1.06$ kPa, $P_{H_2} = 0.64$ kPa, $f_m = 32 \times 10^{-5}$ mol/s.

It is worth emphasizing that non-Faradaic rate changes were obtained only in alkaline solutions. A separate set of experiments in acidic solutions (0.1 M H_2SO_4) gave open-circuit catalytic rates up to a factor of 2 higher than those measured in 0.1 M KOH and only Faradaic rate changes. The latter must be due to the significantly larger (typically a factor of 10 for overpotentials above 0.8 V) electrocatalytic activity we measured in acidic solutions in conjunction with eq 2.

4. Discussion

The present results show that the effect of non-Faradaic electrochemical modification of catalytic activity[1−16] or electrochemical promotion[23] is not limited to solid electrolytes but can also be induced using aqueous KOH and LiOH solutions. Most of the observed features are identical with those observed in NEMCA studies of metal catalyst films deposited on solid electrolytes. These features are the following.

1. The magnitude of the absolute value $|\Lambda|$ of the Faradaic efficiency Λ can be predicted (Table 1) by eq 2, i.e.,

$$|\Lambda| \approx 2Fr_c^o/I_o \tag{2}$$

2. The magnitude of the catalytic rate relaxation constant τ is in good qualitative agreement (Figure 3) with

$$\tau \approx 2FN/I \tag{26}$$

where N is the Pt catalyst surface area (in mol Pt) and I is the applied current. This shows that the observed catalytic rate enhancement (promotion) is due to an electrochemically generated promoting species.

3. There exist catalyst potential E_{rhe} ranges where the catalytic rate varies exponentially with E_{rhe} (Figures 5a and 6a).

4. The apparent activation energy E_a of the catalytic reaction varies linearly with catalyst potential (Figure 14). This, in conjunction with the observed linear variation in the log of the apparent preexponential factor with E_{rhe} (Figure 14), leads to the appearance of the well-known catalysis compensation effect (Figure 13).

In order to rationalize the above general features as well as all the other experimental observations presented in the Results section, the following issues need to be addressed: (I) the nature of the double layer over the liquid-covered and gas-exposed electrode surface; (II) The main charge transfer (electrocatalytic) and catalytic reactions taking place in these two regions; (III) The effect of catalyst−electrode potential on the binding strength of chemisorbed reactants and intermediates and thus on the catalytic activity over the two regions.

Structure of the Double Layer. As previously noted, the kinetic results strongly indicate that the catalytic reaction proceeds via chemisorbed oxygen and hydrogen adatoms, O_{ad} and H_{ad}, respectively, which compete for surface sites with adsorbed hydroxyl groups OH_{ad}. These species are directly adsorbed on the catalyst electrode surface and thus constitute the inner Helmholz plane (IHP). Since the chemisorptive bonds of these species are polar, these species are partly ionized, i.e., $O^{\delta-}$, $OH^{\delta-}$, $H^{\delta+}$, and are accompanied by their compensating (screening) charge in the metal. Solvated K^+ or Li^+ cations are expected to be present at the outer Helmholz plane (OHP).[47,48]

Increasing KOH or LiOH concentration in the solution increases the cation concentration at the OHP and thus the $OH^{\delta-}$ coverage on the electrode surface. This must be the main reason for the observed significant decrease in the open-circuit catalytic rate with increasing KOH concentration (Figure 15).

On the basis of the work of Hansen, Kolb, and co-workers with emersed electrodes,[41−44] it is reasonable to expect that the structure of this double layer is maintained, more or less unperturbed, over the gas-exposed electrode surface as well. In this region, however, owing to the absence of any contacting electrolyte, the rate of the electrocatalytic reactions is negligible. This can explain directly the observed pronounced decrease in current without any appreciable change in catalytic activity upon increasing the gaseous flow rate and thus the fraction, f, of the gas-exposed electrode surface (Figure 11).

The above observation, i.e., significant (6-fold) change in electrocatalytic activity (which is proportional to $l - f$) with changing f without any measurable change in *catalytic* rate, shows that the observed pronounced variation in catalytic rate with potential cannot be attributed, at least for the present system, to possible changes in f due to electrocapillary phenomena[33,54] with varying potential. Such effects may affect f and thus the electrocatalytic activity but not the catalytic activity as observed experimentally.

Electrocatalytic and Catalytic Reactions. As previously noted, two net charge transfer (electrocatalytic) reactions take place on the liquid-covered surface of the Pt electrode:

$$H_2 + 2OH^- \xrightarrow{r_{e,1}} 2H_2O + 2e^- \tag{12}$$

$$2OH^- \xrightleftharpoons{r_{e,2}} (1/2)O_2 + H_2O + 2e^- \tag{13}$$

Over the potential range of the present investigation (0−2.5 V with respect to the r.h.e.), reaction 12 always proceeds to the right ($r_{e,1} > 0$) whereas reaction 13 proceeds to the right when $E_{rhe} > 1.3$ V (Figure 7b). For both reactions the deelectronation of OH^- plays a central role:

$$Pt + OH^- \rightarrow PtOH + e^- \tag{27}$$

Adsorbed OH competes for surface sites with adsorbed H and O adatoms formed from gaseous and/or dissolved H_2 and O_2:

$$H_2 + 2Pt \rightarrow 2PtH \tag{28}$$

$$O_2 + 2Pt \rightarrow 2PtO \tag{29}$$

Adsorbed H and O adatoms can form adsorbed OH as the first step for the catalytic production of H_2O:

$$PtH + PtO \rightarrow PtOH + Pt \tag{30}$$

$$PtOH + PtH \rightarrow H_2O + 2Pt \quad (31)$$

Thus reactions 28−31 constitute the catalytic route for H_2 oxidation.

The electrocatalytic route must involve primarily the direct reaction of OH^- with adsorbed H:[30,49]

$$PtH + OH^- \rightarrow H_2O + Pt + e^- \quad (32)$$

At sufficiently anodic potentials OH^- can also form adsorbed oxygen (Pt "oxide") via the elementary steps leading to oxygen evolution:[30,31]

$$PtOH + OH^- \leftrightharpoons PtO^- + H_2O \quad (33)$$

$$PtO^- \leftrightharpoons PtO + e^- \quad (34)$$

$$PtO \leftrightharpoons Pt + 1/2O_2 \quad (35)$$

The reverse of reactions 33−35 are expected to take place when E_{rhe} is below 1.3 V, thus leading in conjunction with the charge-transfer reaction 32 to a corrosion-type mechanism for H_2O production.

As previously noted (Figure 7b), this corrosion-type mechanism can account for less than 30% of the total rate of H_2 oxidation, in agreement with results obtained in PtO reduction studies.[30,49]

Faradaic Efficiency Λ. The measured Λ values are in good qualitative agreement with

$$|\Lambda| \approx 2Fr_c^\circ/I_o \quad (2)$$

The derivation of the approximate eq 2 has been presented in detail previously.[7] This important relationship shows that a necessary, and as far as we know sufficient, condition for obtaining $|\Lambda|$ values in excess of unity (NEMCA effect) is that the open-circuit *catalytic* rate r_c° must be higher than the parameter $I_o/2F$, which provides a direct measure of the equal and opposite open-circuit charge-transfer (electrocatalytic) rates at the electrode−electrolyte interface. Consequently, the fact that r_c° is higher in the present case than the measured $I_o/2F$ values (Table 1) and also higher than the rate of the above corrosion-type mechanism of H_2 oxidation (Figure 7b) fits nicely with the observed non-Faradaic rate enhancement.

As recently shown,[14] the Faradaic efficiency Λ has an additional interesting physical meaning for oxidation reactions and when $\Lambda \gg 1$. It expresses the ratio of the rate of reaction of the oxidizable species, i.e., H_2, with oxygen chemisorbed on the promoted surface to the rate of the reaction of H_2 with the electrochemically supplied ion, i.e., OH^- in the present case, i.e., the ratio of the rates of reactions 30 and 32. This ratio is significantly higher than unity as previously noted. This again fits nicely with the observed non-Faradaic rate enhancement, i.e., with $\Lambda \gg 1$.

The lack of any non-Faradaic rate enhancement in acidic solutions (0.1 M H_2SO_4) with the catalyst investigated here can be attributed to the very high electrocatalytic activity in these media. Indeed, a series of experiments in the presence of H_2 and O_2 in 0.1 M H_2SO_4 showed that in this case the electrocatalytic activity ($I/2F$) at overpotentials above 0.5V is a factor of 10 higher than in 0.1 M KOH, which in view of eq 2 explains the observed Faradaic behavior.

Origin of NEMCA in Aqueous Solutions. Previous NEMCA studies of metal catalyst−electrodes interfaced with solid electrolytes have shown that the observed non-Faradaic rate enhancement is due to the potential-induced and controlled migration (back-spillover) of promoting ions (e.g., $O^{\delta-}$, $Na^{\delta+}$) on the gas-exposed catalyst surface where they establish an "effective" electrochemical double layer[8,16] and cause a pronounced change in the catalyst surface work function and in the binding strength of chemisorbed reactants and intermediates. The present results and in particular the observed variation in the rate maxima with respect to P_{H_2} and P_{O_2} with catalyst potential (Figures 8−10) show that this is also the case here. Actually, in view of the previous work with emersed electrodes[41−44] it is obvious that the "effective" electrochemical double layer is always present over the gas-exposed electrode surface, and thus no ion migration (back-spillover) is necessary to account for its formation.

The remaining issue is thus to examine the effect of changing catalyst potential E_{rhe} on the work function $e\Phi$ of the catalyst electrode surface and on the chemisorptive bond strength of reactants and intermediates.

As previously noted, the catalyst−electrode surface area A consists of two distinct parts, a gas-exposed part with surface area fA and a liquid-exposed part with surface area $(1 - f)A$ (Figure 12). The Fermi level E_F, or electrochemical potential of electrons $\bar{\mu}$ ($=E_F$)[50] in the Pt catalyst−electrode, is the same in both regions. When the catalyst−electrode potential E_{rhe} is varied by ΔE_{rhe}, $\bar{\mu}$ also changes by

$$\Delta\bar{\mu} = -e\Delta E_{rhe} \quad (36)$$

The work function values $e\Phi_G$ and $e\Phi_L$ over the gas- and liquid-exposed catalyst areas, respectively, are related to $\bar{\mu}$ via

$$-\bar{\mu} = e\Phi_G + e\Psi_G = e\Phi_L + e\Psi_L \quad (37)$$

where Ψ_G and Ψ_L are the outer (Volta) potential over the gas- and liquid-exposed surfaces, respectively. It thus follows from eqs 36 and 37 that

$$e\Delta E_{rhe} = \Delta(e\Phi_G) + e\Delta\Psi_G = \Delta(e\Phi_L) + e\Delta\Psi_L \quad (38)$$

Since the gas phase contains no charge carriers, it follows from simple electrostatics[7] that no net charge can be sustained on the gas-exposed catalyst surface. Thus, $\Psi_G = \Delta\Psi_G = 0$ [7] and eq 38 simplifies to

$$e\Delta E_{rhe} = \Delta(e\Phi_G) \quad (39)$$

which is the same as that derived[7] and experimentally confirmed[3,21] in solid-state electrochemistry. It is worth noting that $e\Phi_G$ also equals one of the four absolute electrode potentials discussed by Trasatti,[51,52] i.e., the one where the reference state is an electron at its ground state and "infinite" distance from the electrode.[51]

Previous work of Hansen, Kolb, and others[41−44,53] has shown that the double layer of emersed electrodes retains its basic features and in fact that eq 39 is also satisfied in aqueous electrochemistry where ΔE_{rhe} is the previously applied overpotential in the immersed state and $\Delta(e\Phi_G)$ is the work function change in the emersed state induced by the previously applied overpotential. Consequently, one may view the gas- and liquid-covered electrode surfaces of the present work as similar to the emersed and immersed state of electrodes in the work Hansen, Kolb, Kötz, Neff, Doblhofer, and co-workers.[41−44,53] Since this work has shown that the double layer structure is very similar in the immersed and emersed state, it is reasonable to assume that eq 39 is also approximately valid for the liquid-covered electrode surface area, i.e.,

$$e\Delta E_{rhe} \approx \Delta(e\Phi_L) \quad (40)$$

Strickly speaking, eq 40 follows from eq 38 only if $e\Delta\Psi_L = 0$, which is expected to hold if the thickness of the diffuse layer is not affected significantly by the applied potential change, which is a reasonable assumption.[32,33] In this case $e\Phi_L$ is the work function one would measure at the end of the diffuse layer and equals the *real* potential of electrons in the metal as discussed by Reiss.[50] On the basis of eqs 34 and 40, one may thus conclude that both $e\Phi_G$ and $e\Phi_L$ increase/decrease with increasing/decreasing E_{rhe}.

In the case of $e\Phi_G$ its linear variation with eE_{rhe} is well established,[7,41−44,53] while in the case of $e\Phi_L$ there is considerable uncertainty over the exact magnitude of the variation. On the basis of the work of Samec, Johnson, and Doblhofer,[53] differences between $e\Phi_G$ and $e\Phi_L$ up to 0.3 V can be expected depending on the nature of the electrolyte.

Regardless of the exact magnitude of the variation in $e\Phi_L$, one can account for the observed pronounced catalytic enhancement by the same simple rule used to rationalize all solid-state electrochemistry NEMCA studies: increasing E_{rhe} causes an increase in $e\Phi_G$ and $e\Phi_L$ and thus a weakening in the chemisorptive bond strength of covalently bonded electron acceptors ($O^{\delta-}$, $OH^{\delta-}$) and a strengthening in the chemisorptive bond strength of covalently bonded electron donors ($H^{\delta+}$). This implies that upon increasing E_{rhe} the adsorption equilibrium constant K_O decreases while K_H increases (Figures 8−10). This electrochemically controlled variation in the binding strength of chemisorbed reactants is the cause of the observed pronounced catalytic rate modification.

5. Conclusions

The catalytic rate of H_2 oxidation on Pt electrodes immersed in alkaline solution is affected significantly and reversibly upon varying the catalyst−electrode potential. The induced change in catalytic rate is up to 100 times larger than the induced change in electrocatalytic rate and up to 5 times larger than the open-circuit catalytic rate. This non-Faradaic rate enhancement is due to the effect of changing catalyst potential on the work function and chemisorptive properties of the Pt surface. This demonstration of electrochemical promotion, or NEMCA effect, in aqueous electrolyte systems may be of considerable importance. It is worth emphasizing, however, that a necessary condition for obtaining non-Faradaic rate enhancements is that the open-circuit *catalytic* rate must be higher than the exchange electrocatalytic rate $I_0/2F$ of the metal−electrolyte interface. Thus, owing to the generally slow kinetics of heterogeneous catalytic reactions at the low temperatures of aqueous electrochemistry, this novel phenomenon may be limited to a few, fast catalytic reactions.

References and Notes

(1) Vayenas, C. G.; Bebelis, S.; Neophytides, S. *J. Phys. Chem.* **1988**, *92*, 5083.
(2) Bebelis, S.; Vayenas, C. G. *J. Catal.* **1989**, *118*, 125.
(3) Vayenas, C. G.; Bebelis, S.; Ladas, S. *Nature (London)* **1990**, *343*, 625.
(4) Politova, T. I.; Sobyanin, V. A.; Belyaev, V. D. *React. Kinet. Catal. Lett.* **1990**, *41*, 321.
(5) Vayenas, C. G.; Neophytides, S. *J. Catal.* **1991**, *127*, 645.
(6) Vayenas, C. G.; Bebelis, S.; Despotopoulou, M. *J. Catal.* **1991**, *128*, 415.
(7) Vayenas, C. G.; Bebelis, S.; Neophytides, S.; Lintz, H.-G. *Catal. Today* **1992**, *11*, 303.
(8) Cavalca, C. A.; Larsen, G.; Vayenas, C. G.; Haller, G. L. *J. Phys. Chem.* **1993**, *97*, 6115.
(9) Chiang, P. C.; Eng, D.; Stoukides, M. *J. Catal.* **1993**, *139*, 683.
(10) Vayenas, C. G.; Ladas, S.; Bebelis, S.; Yentekakis, I. V.; Neophytides, S.; Jiang, Y.; Karavasilis, Ch.; Pliangos, C. *Electrochim. Acta* **1994**, *39*, 1849.
(11) Yentekakis, I. V.; Moggridge, G.; Vayenas, C. G.; Lambert, R. M. *J. Catal.* **1994**, *146*, 292.
(12) Harkness, I. R.; Lambert, R. M. *J. Catal.* **1995**, *152*, 211.
(13) Varkaraki, E.; Nicole, J.; Plattner, E.; Comninellis, Ch.; Vayenas, C. G. *J. Appl. Electrochem.* **1995**, *25*, 978.
(14) Pliangos, C.; Yentekakis, I. V.; Verykios, X. E.; Vayenas, C. G. *J. Catal.* **1995**, *154*, 124.
(15) Yentekakis, I. V.; Vayenas, C. G. *J. Catal.* **1994**, *149*, 238.
(16) Vayenas, C. G.; Jaksic, M. M.; Bebelis, S.; Neophytides, S. In *Modern Aspects of Electrochemistry*; Bockris, J. O.'M., Conway, B. E., White, R. E., Eds.; Plenum Press: New York, 1995; Vol. 29, pp 57−202.
(17) Neophytides, S.; Vayenas, C. G. *J. Phys. Chem.* **1995**, *99*, 17063.
(18) Ladas, S.; Kennou, S.; Bebelis, S.; Vayenas, C. G. *J. Phys. Chem.* **1993**, *97*, 8845.
(19) Palermo, A.; Lambert, R. M.; Yentekakis, I. V.; Vayenas, C. G. *Ionics* **1995**, *1*.
(20) Basini, L.; Cavalca, C. A.; Haller, G. L. *J. Phys. Chem.* **1994**, *98*, 10853.
(21) Ladas, S.; Bebelis, S.; Vayenas, C. G. *Surf. Sci.* **1991**, *251−252*, 1062.
(22) Jiang, Y.; Kaloyannis, A.; Vayenas, C. G. *Electrochim. Acta* **1993**, *38*, 2533.
(23) Pritchard, J. *Nature* **1990**, *342*, 592.
(24) Bebelis, S.; Vayenas, C. G. *J. Catal.* **1992**, *138*, 588.
(25) Bockris, J. O'M.; Minevski, Z. S. *Electrochim. Acta* **1994**, *39*, 1471.
(26) Despic, A.; Drazic, D.; Mihailovic, M.; Lorenz, L.; Adzic, R.; Ivic, M. *J. Electroanal. Chem.* **1979**, *100*, 913.
(27) Baltruschat, H.; Anastasijevic, N. A.; Beltowska-Brzezinska, M.; Hambitzer, G.; Heitbaum, J. *Ber. Bunsen-Ges. Phys. Chem.* **1990**, *94*, 996.
(28) Anastasijevic, N. A.; Baltruschat, H.; Heitbaum, J. *Electrochim. Acta* **1993**, *38*, 1067.
(29) Neophytides, S. G.; Tsiplakides, D.; Stonehart, P.; Jaksic, M. M.; Vayenas, C. G. *Nature (London)* **1994**, *370*, 45.
(30) Conway, B. E. In *Electrodes of Conductive Metal Oxides*; Trasatti, S., Ed.; Elsevier: Amsterdam, 1981; Chapter 9.
(31) Conway, B. E.; Tilak, B. V. *Adv. Catal.* **1992**, *38*, 1.
(32) Bockris, J. O' M.; Reddy, A. K. N. In *Modern Electrochemistry*; Plenum: New York, 1973.
(33) Bockris, J. O' M.; Khan, S. U. M. In Surface Electrochemistry, A Molecular Level Approach; Plenum: New York, 1993; Chapter 3.
(34) Monroe, D. R.; Merrill, R. P. *J. Catal.* **1980**, *65*, 461.
(35) Campbell, C. T.; Ertl, G.; Kuipers, H.; Segner, J. *Surf. Sci.* **1981**, *107*, 220.
(36) Norton, P. R. In *The Chemical Physics of Solid Surfaces and Heterogeneous Catalysis*; King, D. A., Woodruff, D. P., Eds.; Elsevier: Amsterdam, 1982; p 27.
(37) Ceyer, S. T.; Guthrie, W. L.; Lin, T.-H.; Somorjai, G. A. *J. Chem. Phys.* **1983**, *78*, 6982.
(38) Ljungström, S.; Kasemo, B.; Rosén, A.; Wahnström, T.; Fridell, E. *Surf. Sci.* **1989**, *216*, 63.
(39) Hellsing, B.; Kasemo, B.; Zhdanov, V. P. *J. Catal.* **1991**, *132*, 210.
(40) Zhdanov, V. P. *Surf. Sci.* **1993**, *296*, 261.
(41) Hansen, W. N.; Wang, C. L.; Humphreys, T. W. *J. Electroanal. Chem.* **1978**, *90*, 137; **1978**, *93*, 87.
(42) Rath, D. L.; Kolb, D. M. *Surf. Sci.* **1981**, *109*, 641.
(43) Kötz, R.; Neff, H.; Müller, K. *J. Electroanal. Chem.* **1986**, *215*, 331.
(44) Kolb, D. M. *Z. Phys. Chem. (Munich)* **1987**, *154*, 179.
(45) Cremer, E. *Adv. Catal.* **1955**, *7*, 75.
(46) Schwab, G.-M. *J. Catal.* **1983**, *84*, 1.
(47) Gileadi, E. In *Electrode Kinetics for Chemists, Chemical Engineers and Material Scientists*; VCH Publishers: New York, 1993.
(48) Tarasevich, M. R.; Sadkowski, A.; Yeager, E. In *Comprehensive Treatise of Electrochemistry*; Plenum Press: New York, 1987; Vol. 7.
(49) Shibata, S.; Sumino, M. P. *Electrochim. Acta* **1975**, *20*, 739.
(50) Riess, H. *J. Phys. Chem.* **1985**, *89*, 3783.
(51) Trasatti, S. *Electrochim. Acta* **1990**, *35*, 269.
(52) Trasatti, S. *Electrochim. Acta* **1991**, *36*, 1659.
(53) Samec, Z.; Johnson, B.; Doblhofer, K. *Surf. Sci.* **1992**, *264*, 440.
(54) Murphy, O. J.; Wainwright, J. S. *J. Electrochem. Soc.* **1988**, *135*, 138.

JP960971U